Interbasin differences in ocean ventilation in response to variations in the Southern Annular Mode

Darryn W. Waugh[1], Kial Douglas Stewart[2], Andrew McC. Hogg[2], and Matthew H. England[3]

[1]Johns Hopkins University
[2]Australian National University
[3]University of New South Wales

November 26, 2022

Abstract

The response of the ventilation of mode and intermediate waters to abrupt changes in the Southern Annular Mode (SAM) is examined by analyzing the ideal age in a global ocean-sea ice model. The age response is shown to differ between the central Pacific Ocean and other basins. In the central Pacific there are large decreases in the age of subtropical mode and intermediate waters associated with a more positive SAM, contrasting only small age changes in the Atlantic and Indian Oceans, except near where intermediate water density surfaces outcrop. These interbasin differences hold for simulations at different horizontal resolutions, and can be explained by the combination of zonal variations in wind stress changes associated with the SAM, and differences in the age response to an increase or shift in the wind stress. These results suggest that the carbon and heat uptake associated with the SAM will likely vary between ocean basins.

1

1   **Interbasin differences in ocean ventilation in response to variations in the**
2   **Southern Annular Mode**
3
4   Darryn W. Waugh[1,2*], Kial Stewart[3], Andrew McC. Hogg[3], and Matthew H. England[4]
5
6   [1]*Department of Earth and Planetary Sciences*, *Johns Hopkins University*, *Baltimore, MD*
7   [2]*School of Mathematics and Statistics, University of New South Wales, Sydney, New South*
8   *Wales, Australia*
9
10   [3]*Research School of Earth Sciences, and ARC Centre of Excellence for Climate Extremes,*
11   *Australian National University, Canberra, Australian Capital Territory, Australia*
12
13   [4]*Climate Change Research Centre, and ARC Centre of Excellence for Climate Extremes,*
14   *University of New South Wales, Sydney, New South Wales, Australia*
15
16   Corresponding author: Darryn Waugh (waugh@jhu.edu)

17   **Key Points:**

18   • Ventilation of southern oceans in response to changes in the Southern Annular Mode
19   differs between the Pacific Ocean and other basins.
20   • Large decreases in the ideal age occur in the central Pacific for positive Southern Annular
21   Mode but much smaller changes elsewhere.
22   • The interbasin differences are due to zonal variations in the wind together with differing
23   ocean responses to increases or shifts in winds.

24

25 **Abstract**

26 The response of the ventilation of mode and intermediate waters to abrupt changes in the Southern
27 Annular Mode (SAM) is examined by analyzing the ideal age in a global ocean-sea ice model. The
28 age response is shown to differ between the central Pacific Ocean and other basins. In the central
29 Pacific there are large decreases in the age of subtropical mode and intermediate waters associated
30 with a more positive SAM, contrasting only small age changes in the Atlantic and Indian Oceans,
31 except near where intermediate water density surfaces outcrop. These interbasin differences hold
32 for simulations at different horizontal resolutions, and can be explained by the combination of
33 zonal variations in wind stress changes associated with the SAM, and differences in the age
34 response to an increase or shift in the wind stress. These results suggest that the carbon and heat
35 uptake associated with the SAM will likely vary between ocean basins.

36

37 **Plain Language Summary**

38
39 The transport of water from the surface into the interior ocean (ocean "ventilation") is an important
40 process in controlling the amount of heat and carbon that is absorbed by the oceans, with impacts
41 on the global climate. We use an ocean – sea ice model to examine how the time scale for the
42 ventilation of the southern subtropical oceans varies with the leading mode of variability of
43 southern hemisphere climate, the so called Southern Annular Mode (SAM). It is shown that there
44 are significant differences between the Pacific Ocean and other basins. In the Pacific there are
45 large decreases in the ventilation time associated with a more positive SAM, but only small
46 changes in the Atlantic and Indian Oceans. This result suggest that the carbon and heat uptake
47 associated with the SAM will likely also vary between ocean basins. The results hold for
48 simulations at different horizontal resolutions, and can be explained by the combination of zonal
49 variations in wind stress changes associated with the SAM, and differences in the ventilation
50 response to an increase or shift in the wind stress.
51
52

1 Introduction

The Southern Annular Mode (SAM) is the dominant mode of circulation variability in southern mid and high latitude atmosphere and oceans (e.g., Thompson and Wallace 2000, Marshall et al. 2004), and there has been a positive trend in SAM over the last four decades (e.g., Thompson and Solomon 2002). Associated with this trend there has been an intensification and poleward shift of the zonally averaged westerly winds during summer, which is linked to a range of changes in the ocean circulation, including enhanced Ekman transport with increased upwelling in mid-latitudes and downwelling at high latitudes (e.g., Hall and Visbeck 2002; Sen Gupta and England 2006), and an increase, via Sverdrup balance, in the horizontal circulation and strength of the subtropical gyres (e.g., Cai et al. 2006, Roemmich et al. 2007). These changes in ocean circulation then have an impact on the ocean heat and carbon content, the Antarctic Circumpolar Current, ventilation ages, and mode water properties (e.g., Boning et al 2008, Cai et al. 2010, Le Quéré et al., 2007, Waugh et al. 2013, Ting and Holzer 2017, Gao et al. 2018).

Although changes in a wide range of ocean aspects have been linked to changes in SAM, a quantitative relationship is generally lacking. Furthermore, much of the focus has been on changes in zonally averaged winds and ocean circulation: While the SAM is predominantly zonally symmetric there are zonal variations in the strength and meridional structure of the westerly winds associated with SAM during winter (e.g., Codron 2007, Fogt et al. 2012) that could introduce zonal asymmetries in the oceanic response. Zonal asymmetry arguably has a greater impact on the ocean than in the atmosphere, owing to the nature of circulation within closed ocean basins north of $35°S$, and the strong bathymetric steering of flow in the ACC via conservation of potential vorticity.

Here we examine the zonally-varying impact of the SAM on the ventilation of Subantarctic Mode Water (SAMW) and Antarctic Intermediate Water (AAIW). The ventilation of these waters is an important control of the ocean uptake of heat and carbon as well as ocean nutrients (e.g. Frolicher et al. 2015), and knowledge of the ventilation response to SAM will shed light on the potential impact on these processes. The ventilation within the model is quantified using the ideal age, which is not only a fundamental measure of the ventilation but also can be used as a proxy for changes in ocean heat or carbon uptake (e.g. Russell et al. 2006).

Several previous modeling studies have examined the change in ideal age for an increase and poleward shift in the wind stress, either in response to increased atmospheric CO_2 (e.g., Bryan 2006, Ganadesikan et al. 2007) or due to idealized wind perturbations (e.g., Farneti and Gent 2011, Waugh 2014, Waugh et al. 2019). These studies have shown a general decrease in the ideal age (i.e. more rapid ventilation) in SAMW/AAIW when there is an increase and poleward shift in the wind. However, they have considered only the zonal-mean age response or zonally symmetric wind perturbations. As discussed above the changes in the wind stresses accompanying a change in SAM are not zonally uniform, but the impact of these zonal variations on the age response has not been examined. This is the focus of this study.

We examine the age response in a suite of ocean-sea ice model simulations with an abrupt change in the atmospheric forcing from a year with neutral SAM to a year with extreme anomalous positive or negative SAM (Stewart et al 2020a). These abrupt change in forcing simulations enable the response to be a particular anomalous SAM to be isolated. It is difficult to isolate the response to a particular SAM event from simulations with interannually varying forcing, as the response time for the ideal age to changes in atmospheric forcing is multiple decades and ocean changes

96 are due to the time-integrated (weighted) change in the atmospheric forcing (Waugh and Haine
97 2020) and hence to several different phases of SAM.

98 The model simulations analyzed and methods used are described in the next Section. Then,
99 before examining the perturbation experiments, we quantify in Section 3 the relationships between
100 SAM and wind stress over the southern oceans. The zonal-mean age response is examined in
101 Section 4, while regional variations (in particular, differences between oceans) are examined in
102 Section 5. Concluding remarks are in the final section.

103

104

105 **2. Model and Methods**
106 We examine a suite of simulations using the Australian Community Climate and Earth System
107 Simulator, ocean model version 2 (ACCESS-OM2) global ocean-sea ice model (Kiss et al. 2020)
108 where atmospheric forcing for different 12-month periods from the Japanese 55-year atmospheric
109 reanalysis data-set for driving ocean models (JRA55-do, Tsujino et al., 2018) are used repeatedly
110 to drive the model (Stewart et al 2020a). This suite includes simulations using 12-month periods
111 previously identified as globally climatically-neutral periods suitable for extended simulations
112 without interannual variability or substantial model drift (Stewart et al., 2020b), as well as 12-
113 month periods with extremely anomalous (positive and negative) Southern Annular Mode (SAM)
114 conditions (Stewart et al. 2020a). The latter are referred to as "SAM+ years" (for extreme positive
115 SAM periods) and "SAM- years".
116 These simulations have been performed at three different resolutions (nominal horizontal
117 resolution of 1°, 0.25° and 0.1°. We focus here on the 1° version as three different reference year
118 simulations have been performed, and for each there are six perturbation simulations (three SAM+
119 and three SAM-). For the higher resolution simulations there is only a single reference case, and
120 four SAM perturbations (two SAM+ and two SAM-) (Stewart et al. 2020a).
121 The 1° version of ACCESS-OM2 has a horizontal grid spacing of (nominally) 1° latitude
122 and longitude, and 50 unevenly spaced vertical levels in a z* generalized vertical coordinate. The
123 vertical grid spacing increases smoothly with depth from 2.3m at the surface to ~220m at ~3000m
124 (maximum depth of ~5400m), designed to support the vertical structure of mode-1 baroclinic
125 processes (Stewart et al. 2017). See Kiss et al (2020) for additional model details and evaluation.
126 Reference year simulations with the 1° model version have been performed with 12-month
127 (May to April of the following year) periods from 1984/85, 1990/91 and 2003/04 (referred to as
128 RYF8485, RYF9091 and RYF0304). These simulations were initialized with January temperature
129 and salinity fields from the World Ocean Atlas 2013 (WOA13; Locarnini et al., 2013; Zweng et
130 al., 2013) and run for 600 years. For each of the three 600-year RYF simulations, eight 300-year
131 perturbations are branched off at the model year 300. Two of these perturbations correspond to the
132 other two RYF periods and six correspond to SAM periods: The SAM+ years are 1998/99, 2010/11
133 and 2015/16 (referred to as SAM+9899, SAM+1011, and SAM+1516, respectively), and the
134 SAM- years are 1991/92, 2003/04 and 2016/17 (referred to as SAM-9192, SAM-0304 and SAM-
135 1617, respectively). In these perturbation simulations the atmospheric forcing fields used to
136 calculate air-sea fluxes are abruptly changed from the RYF to the different forcing without
137 smoothing. This approach grants a total of 27 simulations; 3x 600-year RYF simulations, and 24x
138 300-year perturbation simulations.
139 The three RYF periods and six extreme SAM periods represent nine different forcing years
140 with a range of SAM conditions. The three RYF periods, while not identified based on the
141 neutrality of SAM alone, have near neutral SAM indices. This is evident in the latitudinal variation

142   of anomalies in (a) sea-level pressure and (b) zonal-mean winds, shown in **Figure 1**. The three
143   reference years (green curves) generally have small anomalies in SLP and winds. The SAM+ years
144   (red) have positive SLP anomalies at lower latitude and negative SLP anomalies at high latitudes,
145   which correspond to positive wind anomalies south of 45°S. The SAM- years (blue) generally have
146   the opposite SLP and wind anomalies to the positive years. The years RYF8485 and SAM-1617
147   do not fit exactly in the above characterization, as the SAM anomaly for RYF8485 (SAM=-0.37)
148   is more negative than SAM-1617 (SAM=-0.10).
149   All simulations include an ideal age tracer diagnostic (or "age" for short). This tracer is set
150   to zero in the model surface level (which is 2.3m thick) at each time step, increases by 1 yr yr^{-1}
151   within the ocean interior, and is advected and diffused as other tracers (e.g., temperature and
152   salinity). In the limit of long times compared to the circulation, the ideal age equals the mean time
153   since water last made surface contact (e.g., England 1995, Hall and Haine 2002). Waugh et al.
154   (2019) examined the change in ideal age in wind stress perturbation simulations with an early
155   (0.25°) version of MOM.
156   We focus on the age distribution for $\sigma_2 < 36.5$ kg/m^3, which includes SAMW and AAIW,
157   as the ventilation of these waters is particularly important for understanding the ocean uptake of
158   heat and carbon. The majority of our analysis is on fields averaged over the last 10 years of the
159   perturbation simulations (i.e. 290-299 years after the perturbation was applied), and the difference
160   in these average fields from corresponding averaged in the RYF simulations.
161
162   **3. Relationship between SAM and wind stress**
163   The primary mechanism by which changes in SAM are thought to influence the ocean
164   circulation and ventilation is through changes in the wind stress. Therefore, before examining the
165   age in the perturbation experiments described above we quantify the relationship between SAM
166   and zonal wind stress (τ_x). For this analysis we use the SAM index and wind stress for 1979/80 to
167   2016/17 from an ACCESS-OM2 simulation driven by interannual JRA55-do atmospheric state
168   from 1958 to 2017 (IAF; Kiss et al., 2020). This IAF simulation was continuously cycled through
169   five iterations of this forcing dataset, and we analyze the model output from the last cycle. For
170   both SAM and wind stress we examine the annual-mean from 1 May to 30 April the following
171   year.
172   A linear regression analysis between τ_x and SAM shows that there is generally an increase
173   in the τ_x poleward of 45°S (with peak increase around 55°S) and decrease equatorward of 45°S for
174   positive SAM (**Figure 2**). As the climatological peak τ_x at each longitude is around 50-55°S (bold
175   curve), the polar increase and mid-latitude decrease of τ_x corresponds to an increase and poleward
176   shift of the peak zonal-mean τ_x with a more positive SAM. This poleward intensification is shown
177   more clearly in **Figs. 3a,b** which show that both magnitude and latitude of the peak zonal-mean τ_x
178   are highly correlated with SAM (correlation coefficient r=0.9 and r=-0.7, respectively.   There are,
179   however, substantial zonal variations in the latitude of the peak zonal wind stress, with peak values
180   of τ_x over the Pacific poleward of those over the Atlantic and Indian oceans (thick curve in **Fig 2**),
181   and the relationship between SAM and the magnitude and latitude of the peak τ_x varies with
182   longitude.
183   The relationship between the SAM index and the magnitude and latitude of the peak τ_x
184   averaged over the Pacific Ocean (150°E-70°W) and the combined Atlantic and Indian Oceans

185   (60°W-120°E) is quantified in **Figs 3c-f**[1]. The SAM–τ_x relationships differ between the Pacific and

186   Atlantic-Indian Oceans. The magnitude of the peak τ_x averaged over the Pacific is highly

187   correlated with SAM (r=0.9), but there are insignificant correlations between the latitude of the

188   peak τ_x and SAM (r=0.1). In contrast, the latitude and magnitude of the peak Atlantic-Indian τ_x

189   are both correlated with SAM (but slightly weaker than the peak Pacific τ_x). These differences in

190   SAM-τ_x relationships between the Pacific and Atlantic-Indian oceans are consistent with previous

191   studies of the zonal asymmetries in SAM (e.g. Codron 2007, Fogt et al. 2012).

192

193   **4. Zonal-Mean Age Response**

194   The above differences in the SAM – wind stress relationship between basins suggests that the

195   ocean response to SAM could vary between basins. However, before examining the age response

196   in different basins we first examine the zonal-mean age response, principally to allow comparison

197   with previous studies examining the zonal-mean age response to changes in wind stress.

198   **Figure 4** shows that there are substantial changes in the zonal-mean age response ($\Delta\bar{a}$) for

199   the SAM+ and SAM- perturbations from the RYF9091 simulations, with maximum age changes

200   of 30-50%. There is a wide variation in the spatial pattern and sign of $\Delta\bar{a}$: For some perturbations

201   the sign of $\Delta\bar{a}$ is the same throughout nearly all of the mode and intermediate waters (35.5 kg/m^3

202   $< \sigma_2 < 36.5$) (e.g., **Fig 4a,b, f**), while for other perturbations there are both regions of increase and

203   decrease in $\Delta\bar{a}$ within these waters (e.g., **Fig 4d,e).**

204   Much of the variation among the perturbations in $\Delta\bar{a}$ within SAMW and AAIW can be

205   explained by differences in the SAM anomaly (ΔSAM; see value listed at the bottom of each panel

206   in **Fig 4**). There is a decrease in age throughout most of the mode-intermediate waters for

207   perturbations with ΔSAM>0 and an increase in age when ΔSAM<0. However, the SAM anomaly

208   is not the sole determinant, as there are differences between the response for perturbations with

209   the same or similar SAM (e.g. 9899 and 1011). Also, for all perturbations $\Delta\bar{a} < 0$ at the location

210   35°S, 500 m depth ($\sigma_2 = 35.5$ kg/m^3). In this region $\Delta\bar{a}$ is insensitive to ΔSAM.

211   To quantify the change in age associated with SAM we perform a linear regression analysis

212   using $\Delta\bar{a}$ from the perturbation simulations branching off a given RYF simulation and

213   corresponding changes in ΔSAM. That is, at a given latitude (φ) and depth (z), we solve for α_{SAM},

214

215             $\Delta\bar{a}_k(\varphi, z) = \alpha_{SAM}(\varphi, z)\Delta SAM_k + c,$ *(1)*

216

217   where ΔSAM_k is the change in SAM index for the kth perturbation, $\Delta\bar{a}_k$ the age response for

218   corresponding perturbation, c is a constant, and α_{SAM} is the sensitivity of $\bar{a}$ to a unit change in the

219   SAM index. This regression is performed over the perturbations from all three RYF simulations

220   (i.e. over 24 perturbation simulations). As shown in **Fig. 5a**, there is a decrease in $\bar{a}$ with increasing

221   SAM (negative α_{SAM}) throughout AAIW and in lower parts of SAMW. In the upper part of SAMW

222   and lighter waters α_{SAM} is small and there is not a significant correlation between SAM and $\bar{a}$. The

223   largest percentage difference occurs in AAIW around 50-55°S, where $\alpha_{SAM} \sim$ -50% per unit SAM.

---

[1] Analysis of interannual correlations of latitude and magnitude of the peak winds averaged over different oceans shows a high correlation between the Atlantic and Indian Oceans, but only weak interannual correlations between Pacific-average wind stress and wind stress over Atlantic or Indian Oceans.

224   As shown above there is a high correlation between both the change in magnitude of the
225 peak zonal wind stress (τ_{max}) and the change in latitude of this peak (τ_{lat}) with the change in SAM.
226 The decrease in mode and intermediate water age with SAM is therefore consistent with previous
227 studies showing a decrease in age for increased and poleward shifted winds (e.g., Waugh et al.
228 2019). To isolate the role of an increase or shift in the wind stress governing changes in the zonal-
229 mean age we apply a multiple linear regression analysis similar to the above SAM analysis, i.e. at
230 each latitude and depth, we solve for $\alpha_{increase}$ and α_{shift} in the set of equations
231

232    $$\Delta \bar{a}_k(\varphi, z) = \alpha_{increase}(\varphi, z)\Delta\tau_{max,k} - \alpha_{shift}(\varphi, z)\Delta\tau_{lat,k} + c \qquad (2)$$

233

234 where $\Delta\tau_{max,k}$ and $\Delta\tau_{lat,k}$ are changes in magnitude and location of peak wind stress for the kth
235 perturbation, and the quantities $\alpha_{increase}$ and α_{shift} correspond to the sensitivity of the age to an
236 increase and a shift in the peak wind stress, respectively. There is a negative sign before the second
237 term so that a positive α_{shift} indicates the sensitivity to a poleward shift in the peak wind stresses.
238 There is a decrease in age throughout mode and intermediate waters (35.5 kg/m^3 < σ_2 < 36.5) for
239 an increase in the wind stress (**Figure 5b)**. On the other hand, age decreases only poleward of 45°S
240 for a poleward shift in the peak wind stress, and there is (statistically insignificant) increase of age
241 equatorward of 45°S (**Figure 5c)**.
242   The range of τ_{max} across the perturbations is around 0.05 N/m^2 while the range of τ_{lat} is
243 around 3° (see **Fig 3**). Combining these ranges with maximum magnitude of $\alpha_{increase}$ and α_{shift} (15%
244 per 0.01 N/m^2 and 25% per degree, respectively) indicates that the peak changes of $\Delta\bar{a}$ associated
245 with an increase or shift of wind stresses are of similar magnitude. Thus, both the increase and
246 shift of the peak wind stress needs to be considered. Although, as the maximum contributions from
247 an increase or shift in winds occur in different locations, the relative importance of an increase or
248 shift is expected to vary zonally.
249   The spatial patterns of $\alpha_{increase}$, and α_{shift} in **Fig 5** are similar to those from the abrupt wind-
250 stress perturbations shown in Waugh et al. (2019). This similarity also applies to the magnitude of
251 the response. **Figure 6(a,b)** shows the results of the multiple linear regression analysis of
252 RYF9091 perturbations 50 years after the perturbation (to be consistent with the length of the
253 simulations in Waugh et al. (2019)). These results are compared (in **Fig 6c,d**) with Δa from the
254 Waugh et al. (2019) simulations re-expressed as sensitivities $\alpha_{increase}$ and α_{shift}. Note that the
255 smaller magnitude of $\alpha_{increase}$ for 50 years, rather than 300 years after the perturbation, is consistent
256 with decadal-to-century age response time shown in Waugh and Haine (2020). Figure 6 shows
257 good agreement between the estimated and directly simulated (Waugh et al. 2019) sensitivities,
258 including the spatial structure and magnitude of the sensitivities. Note, although the region of
259 positive α_{shift} in Fig 5c is not statistically significant, the direct simulations also shows positive
260 α_{shift} at lower latitudes. The good agreement in **Fig 6** is perhaps surprising given the many
261 differences between the two sets of simulations: The sensitivities in Waugh et al. (2019) come
262 from direct perturbations and not a regression analysis, and the Waugh et al. (2019) simulations
263 have zonally symmetric wind perturbations, with no seasonality, and no changes in other
264 atmospheric properties (e.g., buoyancy fluxes). The overall agreement supports the conclusion that
265 changes in zonal-mean ideal age within southern mode and intermediate waters in response to
266 abrupt change in SAM are consistent with response to changes in magnitude and latitude of the
267 peak zonal-mean wind stress.
268

269 **5. Zonal Variations in Age Response**
270   The above analysis has shown that the zonal-mean ideal age response is consistent with
271 expected changes from the change in zonal-mean wind stress between simulations, however, the
272 analysis in Section 3 shows large differences in the SAM-wind stress relationship between the
273 Pacific and Atlantic-Indian oceans. Thus, differences in the age response between ocean basins
274 may be expected.
275   Substantial zonal variation in the age response at fixed depth are indeed found (see **Figure**
276 **7)**. This variation is not limited to the magnitude of Δa; for many perturbations the sign of Δa
277 changes with longitude. In some simulations the sign of subtropical (30-45°S) central Pacific Δa
278 differs from the subtropical Δa in the Indian and/or Atlantic Oceans (e.g., **Fig 7a,e,f**). In other
279 cases, the sign of the central Pacific Δa differs from that in the Tasman Sea and the eastern
280 boundary of the Pacific Ocean (e.g., **Fig 7c,e**). Furthermore, there is an age decrease in the Tasman
281 Sea for all perturbation simulations (i.e. changes independent of the sign the change in SAM).
282   To quantify these zonal variations, we examined the relationships among 30-45°S Δa
283 averaged over the Central Pacific (170-100°W), Indian (30-120°E), Atlantic (60°W-20°E), Eastern
284 Pacific Oceans (80-70°W), or the Tasman Sea (155-165°E). For Δa at 900 m, there is only a very
285 weak relationship between the Central Pacific Δa and either the Indian or Atlantic Oceans Δa
286 (correlation coefficient, r, equal 0.2 and 0.4 respectively). Further, there is also only a very weak
287 relationship between the Central Pacific Δa and that over the Eastern Pacific or Tasman Sea (r =
288 0.4, 0.2, respectively). In contrast, there is a high correlation between the Indian and Atlantic
289 Ocean Δa (r=0.96), between Indian Ocean and Tasman Sea Δa (r=0.65), and between the Atlantic
290 Ocean and Eastern Pacific Δa (r=0.91).
291   Waugh et al. (2019) showed that much of the zonal-mean age response within SAMW and
292 AAIW can be explained by a change in subtropical gyre transport induced by the change in wind
293 stress curl, consistent with Sverdrup balance. This relationship also applies to the simulations
294 considered here, only now we assess more carefully the inter-basin differences. The changes in
295 barotropic stream function (BSF) calculated from Sverdrup balance for the perturbation from
296 RYF9091 are shown in **Figure 8** and are consistent with many of the features in maps of 900m Δa
297 shown in **Fig 7**. For example, the sign of Δa within the central Pacific is the same as that of the
298 ΔBSF, consistent with an increase in BSF corresponding to a weaker barotropic circulation (the
299 BSF is negative within the southern subtropical gyres) which leads to slower advection of water
300 and older ages. Also, there are generally differences in the pattern (and sign) of ΔBSF in the Pacific
301 from the Atlantic and Indian Oceans, consistent with the differences in Δa between oceans. There
302 are also perturbations where the sign of ΔBSF in the central Pacific differs from the eastern Pacific
303 or Tasman Sea.
304   The differences in Δa between basins are not limited to 900m, but occur throughout mode
305 and intermediate waters. As illustrated in **Fig 9** for a SAM+ and SAM- perturbation, there are large
306 changes in the Central Pacific age in mid-latitude (30-45°S) SAMW and AAIW with SAM, with
307 age increasing (decreasing) by around 30-40% for a decrease (increase) in SAM. In contrast, for
308 age averaged over the Atlantic-Indian Oceans there are only small changes in mid-latitudes that
309 are often of opposite sign from the Central Pacific, and the largest change in the Atlantic-Indian
310 Oceans occur further south in near-surface AAIW.
311   **Figure 9** indicates that the age-SAM relationship is very different between the Central
312 Pacific and Atlantic-Indian average age. To quantify this, we perform the age-SAM linear
313 regression analysis (equation 1) for the basin-average rather than zonal-mean a. As shown in **Fig**

314 **10a,d**, there is negative α_{SAM} (a decrease in age for increase in SAM) for both the Central Pacific
315 and Atlantic-Indian oceans, but the magnitude and spatial structure differs. There are large positive
316 values of Central Pacific α_{SAM} in subtropical SAMW and AAIW (30-50°S, $35.5 < \sigma_2 < 36.5$ kg/m^3)
317 with, and smaller, generally insignificant, values elsewhere. In contrast, α_{SAM} is small
318 (insignificant) for Atlantic-Indian age in this region, and large α_{SAM} are limited to more southern
319 AAIW (~55°S, $\sigma_2 \sim 36.5$ kg/m^3) near the surface (and the decrease in age is smaller, with peak
320 around 30-40% per unit of SAM).
321 　　　The above differences in age response to SAM between basins are consistent with the
322 combination of (i) inter-basins differences in wind stress changes associated with SAM and (ii)
323 the different age response to an increase or shift in peak wind stress. Over the Pacific the magnitude
324 of τ is positively correlated with SAM but there is no correlation between the location of peak τ
325 and SAM (Section 3). We therefore expect the age change associated with SAM in the Pacific
326 Ocean to mirror the response to an increase in wind stress, which is a decrease in age in subtropical
327 SAMW and AAIW waters (Section 4). This decrease is indeed what **Fig 10a** shows. For the
328 Atlantic-Indian Oceans there is both an increase and poleward shift in wind stress associated with
329 positive SAM (Fig 3), and both impact the age. North of 45°S (within 500-1000 m) the age
330 decreases with an increase of the peak wind stress (**Fig 5**) but age increases with a poleward shift,
331 so these wind stress changes cancel each other and little change in a with SAM is expected
332 (consistent with **Fig 10b**). South of 45°S a poleward shift in peak wind stress cause the opposite
333 sign change in age. Thus, both an increase and shift associated with SAM cause a decrease in age,
334 again consistent with **Fig 10b**.
335
336 **6. Resolution Dependence**
337 　　　A possible concern with the results presented above is the low horizontal resolution (1°) of
338 the model, which raises the question as to whether the impact of mesoscale eddies is accurately
339 captured. As described in Section 2, some simulations at 0.25° and 0.1° horizontal resolution have
340 also been performed, and we now use output from these simulations to assess the impact of
341 horizontal resolution on the age response and our key conclusions.
342 　　　For the higher resolution simulations there is only a single (RYF9091) reference case, and
343 the perturbation simulations were branched from year 150 (0.25° resolution) and year 50 (0.1°
344 resolution), rather than year 300 in the 1° resolution (Stewart et al 2020a). Furthermore, only four
345 perturbation simulations were performed, and the 0.1° perturbations were only run for 20 years.
346 Thus, the full analysis described above cannot be repeated for the higher resolution runs. However,
347 the response for individual perturbations can be compared. As there is a decadal to centennial
348 response time for age to wind stress perturbations (Waugh and Haine 2020), it is important to
349 compare simulations are at same stage of the transient response. Thus, we compare simulations 20
350 years (the length of the 0.1° simulations) after the perturbation was applied.   This comparison is
351 shown in **Figure 11** which shows the ideal age response, averaged over the Central Pacific or
352 Atlantic-Indian oceans, for the SAM-9192 and SAM+9899 perturbations from RYF9091, for 1.0°,
353 0.25° and 0.1° resolution simulations. The 1° simulations in **Figure 11** are the same as in **Figure**
354 **9**, but for an earlier response time (20 instead of 300 yrs).
355 　　　The broad scale patterns and magnitude of the response shown in **Figure 11** are the same
356 for all resolutions. In particular, for all resolutions there is a much larger response in the Central
357 Pacific (maximum around 20-30%) than in the Atlantic-Indian Oceans (generally around or less
358 than 5%).

359   There are some differences in detail between the different resolutions, with the most
360   noticeable being a shallower response in the Central Pacific at the higher resolution. The cause of
361   this difference is unclear. It is most likely related to a more realistic, along-isopycnal eddy
362   transport at higher resolution (Stewart et al 2020a). Further research is required to determine the
363   cause of the shallower response at the higher resolution, but this difference does not impact our
364   primary conclusion that the age-SAM relationship differs between the Central Pacific and Atlantic-
365   Indian Oceans.
366   The limited sensitivity of the age response to resolution shown in Figure 11 is consistent
367   with the agreement in the simulated age response to an increase in the zonal-mean winds from 1°
368   coupled climate model (Waugh 2014) and 0.25° ocean-sea ice model (Waugh et al 2019)
369   simulations. Furthermore, it is also consistent with the Waugh et al (2019) result that the change
370   in age can be explained by the change in wind stress curl and linear theory, i.e. age changes due a
371   combination of vertical movement of isopycnals (via Ekman pumping) and changes in horizontal
372   circulation (via Sverdrup balance).
373
374   7. Conclusions
375   Analysis of a suite of abrupt forcing simulations with the ACCESS-OM2 ocean-sea ice
376   model indicates that the response of the ventilation of southern mode and intermediate waters
377   (SAMW/AAIW) to changes in SAM differs between the central Pacific Ocean and other basins.
378   In the Central Pacific there are large decreases in the ideal age in subtropical SAMW/AAIW
379   associated with a more positive SAM, and smaller, generally insignificant, changes elsewhere. In
380   contrast, in the Atlantic-Indian Oceans the age decreases associated with an increase in SAM are
381   small except in more polar, near-surface AAIW. The conclusion that the age response to SAM is
382   much larger in the Central Pacific than in other ocean basins is not sensitive to the horizontal
383   resolution of the simulations, and the holds for simulations at 1°, 0.25° and 0.1°.
384   These inter-basin differences in age response are due to the combination of zonal variations
385   in the changes in wind stress associated with an increase in SAM, together with the different age
386   response to an increase or shift in the peak wind stress. Over the Pacific Ocean the magnitude of
387   the peak wind stress is highly correlated with SAM, but there are insignificant correlations between
388   the latitude of the peak wind stress and SAM. The decrease of age in SAMW and AAIW within
389   the Central Pacific is consistent with this increase in wind stress (with limited shift) associated
390   with SAM. In contrast, both the latitude and magnitude of the peak Atlantic-Indian wind stress are
391   correlated with SAM, and large changes in age are limited to south of 45°S as the increase and
392   poleward shift of the wind stress cause opposing age changes north of 45°N.
393   The atmospheric forcing used for the different SAM+ or SAM- perturbations include
394   differences not only in the wind stress but also in buoyancy fluxes, and changes in buoyancy fluxes
395   could contribute to the differences in age. It is not possible from these simulations to isolate the
396   role of wind versus buoyancy forcing, but the ability of the wind stress changes associated with
397   SAM (and linear theory) to explain the SAMW/AAIW age changes indicates that changes in
398   buoyancy fluxes play only a minor role in the age-SAM relationship. This minor role may not
399   carry over to all aspects of the ocean response, i.e. changes in mixed layer depth and subduction
400   rates are likely more sensitive to SAM-related changes in buoyancy fluxes (Downes et al. 2017,
401   Sallee et al. 2010).
402   One question that follows the above modeling results is whether there is observational
403   evidence for regional variations in ocean ventilation associated with SAM. A direct comparison of
404   the simulations examined here and observations is not possible given that we have analyzed the

405   long-term (steady) response in idealized (unrealistic) abrupt forcing simulations, whereas in reality
406   there are interannual variations in atmospheric forcing and the age responds to the time-integrated
407   changes in wind stress over previous decades (Waugh and Haine 2020). However, the simulations
408   may provide guidance for the age response to the positive trend in SAM over the last four decades.
409   Analysis of repeat measurements of transient tracers in the southern oceans by Waugh et al. (2013)
410   and Ting and Holzer (2017) show a decrease in SAMW age from the early 1990s to mid 2000s
411   within all three ocean basins. This would appear to contradict the model result which indicates
412   there should a substantial decrease of age in subtropical SAMW within the Central Pacific, but
413   much smaller age changes in corresponding water within the Atlantic/Indian Oceans. However,
414   the observational estimates in the Indian and Atlantic Oceans is based on a single section in each
415   ocean (as opposed to 3 in the Pacific) and the estimated changes in age are noisy (less coherent)
416   than in the Pacific Ocean. Furthermore, analysis of a different (zonal) section in the southern Indian
417   Ocean by Álvarez et al (2011) and Tanhua et al. (2013) indicate no long-term change in the age.
418   Thus, it is possible that changes in SAMW age have been much larger across the central Pacific
419   Ocean than averaged over the Indian Ocean. Further analysis required to test this, including
420   analysis of more recent repeat transient tracer measurements.

421   Another area worth pursing is the possible connection between inter-basin differences in
422   the age response to SAM and the oceanic uptake of carbon and heat. For example, Keppler and
423   Landschützer (2019) have shown regional differences in the carbon uptake associated with SAM,
424   and whether this can be explained by the inter-basin differences in wind stress and age
425   relationships with SAM needs to be explored.

431

References

Álvarez, M., Tanhua, T., Brix, H., Lo Monaco, C., Metzl, N., McDonagh, E. L., & Bryden, H. L. (2011). Decadal biogeochemical changes in the subtropical Indian Ocean associated with Subantarctic Mode Water. *Journal of Geophysical Research: Oceans*, *116*(C9).

Böning C. W., Dispert, A., Visbeck, M., Rintoul, S. R. & Schwarzkopf, F. U. 2008: The response of the Antarctic Circumpolar Current to recent climate change. *Nature Geosci.* 1, 864-869.

Bryan, F. O., Danabasoglu, G., Nakashiki, N., Yoshida, Y., Kim, D. H., Tsutsui, J., & Doney, S. C. (2006). Response of the North Atlantic thermohaline circulation and ventilation to increasing carbon dioxide in CCSM3. *Journal of Climate*, *19*(11), 2382-2397.

Cai, W. (2006). Antarctic ozone depletion causes an intensification of the Southern Ocean super-gyre circulation. *Geophysical Research Letters*, *33*(3).

Cai W, Cowan T, Godfrey S, Wijffels S (2010), Simulation of processes associated with the fast warming rate of the southern midlatitude ocean. *J Climate*, 23:197–206

Codron, F. (2007). Relations between annular modes and the mean state: Southern Hemisphere winter. *Journal of the atmospheric sciences*, *64*(9), 3328-3339.

Downes, S. M., C. Langlais, J. P. Brook, & P. Spence (2017). Regional impacts of the westerly winds on Southern Ocean Mode and Intermediate Water subduction. *J. Phys. Oceanogr.*, 47, 2521–2530.

England, M.H., (1995). The age of water and ventilation timescales in a global ocean model. *J Phys. Oceanogr.*, *25*, 2756-2777.

Fogt, R. L., Jones, J. M., & Renwick, J. (2012). Seasonal zonal asymmetries in the Southern Annular Mode and their impact on regional temperature anomalies. *Journal of climate*, *25*(18), 6253-6270.

Frölicher, T. L., Sarmiento, J. L., Paynter, D. J., Dunne, J. P., Krasting, J. P., & Winton, M., (2015). Dominance of the Southern Ocean in Anthropogenic Carbon and Heat Uptake in CMIP5 Models. Journal of Climate, 28(2), 862–886, doi: 10.1175/JCLI-D-14-00117.1.

Farneti, R., and P. R. Gent (2011). The effects of the eddy-induced advection coefficient in a coarse-resolution coupled climate model. Ocean Modell., 39, 135–145, https://doi.org/10.1016/ j.ocemod.2011.02.005.

Gnanadesikan, A., Russell, J. L., & Zeng, F. (2007). How does ocean ventilation change under global warming? Ocean Sci., 3, 43–53.

Gao, L., Rintoul, S.R. & Yu, W., 2018. Recent wind-driven change in Subantarctic Mode Water and its impact on ocean heat storage. *Nature Climate Change*, *8*, 58.

Hall, A. and Visbeck, M., (2002), Synchronous variability in the Southern Hemisphere atmosphere, sea ice, and ocean resulting from the annular mode. *Journal of Climate*, *15*(21), pp.3043-3057

Hall, T.M., & T.W.N. Haine 2002: On Ocean Transport Diagnostics: The Idealized Age Tracer and the Age Spectrum, *J. Phys. Ocean.*, 1987-2001.

Keppler, L., & Landschützer, P. (2019). Regional wind variability modulates the Southern Ocean carbon sink. *Scientific reports*, *9*(1), 1-10.

Kiss, A. E., Hogg, A. McC., Hannah, N., Boeira Dias, F., Brassington, G. B., Chamberlain, M. A., Chapman, C., Dobrohotoff, P., Domingues, C. M., Duran, E. R., England, M. H., Fiedler, R., Griffies, S. M., Heerdegen, A., Heil, P., Holmes, R. M., Klocker, A., Marsland, S. J., Morrison, A. K., Munroe, J., Nikurashin, M., Oke, P. R., Pilo, G. S., Richet, O., Savita, A., Spence, P., Stewart, K. D., Ward, M. L., Wu, F., and Zhang, X., (2020). ACCESS-OM2

478   v1.0: a global ocean–sea ice model at three resolutions, *Geosci. Model Dev.*, 13, 401–442,
479   doi:10.5194/gmd-13-401-2020.
480 Le Quéré, C., Rödenbeck, C., Buitenhuis, E.T., Conway, T.J., Langenfelds, R., Gomez, A.,
481   Labuschagne, C.Ramonet, M., Nakazawa, T., Metzl, N. & Gillett, N. (2007). Saturation of
482   the Southern Ocean CO2 sink due to recent climate change. Science, 316, 1735-1738
483 Marshall, G. J., Stott, P. A., Turner, J., Connolley, W. M., King, J. C., & Lachlan-Cope, T. A.
484   (2004). Causes of exceptional atmospheric circulation changes in the Southern Hemisphere.
485   *Geophysical Research Letters*, *31*(14).
486 Roemmich, D., J Gilson, R. Davis, P. Sutton, S. Wijffels, & S. Riser, (2007). Decadal Spinup of
487   the South Pacific Subtropical Gyre, J. Phys. Ocean., 37, 162.
488 Roemmich, D., Gilson, J., Sutton, P. & Zilberman, N., (2016). Multidecadal change of the South
489   Pacific gyre circulation. *Journal of Physical Oceanography*, *46*(6), pp.1871-1883.
490 Russell, J.L., Dixon, K.W., Gnanadesikan, A., Stouffer, R.J. and Toggweiler, J.R., 2006. The
491   Southern Hemisphere westerlies in a warming world: Propping open the door to the deep
492   ocean. *Journal of Climate*, *19*(24), pp.6382-6390.
493 Sallée, J. B., Speer, K. G., & Rintoul, S. R. (2010). Zonally asymmetric response of the Southern
494   Ocean mixed-layer depth to the Southern Annular Mode. *Nature Geoscience*, *3*(4), 273-279.
495 Sen Gupta, A. and England, M.H., (2006). Coupled ocean–atmosphere–ice response to variations
496   in the southern annular mode. *Journal of Climate*, *19*, 4457-4486
497 Stewart, K. D., Hogg, A. M., Griffies, S. M., Heerdegen, A. P., Ward, M. L., Spence, P., &
498   England, M. H., (2017). Vertical resolution of baroclinic modes in global ocean models.
499   *Ocean Modell.*, 113, 50–65, doi:10.1016/j.ocemod.2017.03.012.
500 Stewart, K. D., Hogg, A. M., England, M. H., and Waugh, D.W., (2020a) Response of the
501   Southern Ocean overturning circulation to extreme Southern Annular Mode conditions,
502   *Geophysical Research Letters*, submitted, doi: 10.1002/essoar.10503406.1
503 Stewart, K. D., Kim, W. M., Urakawa, S., Hogg, A. M. C., Yeager, S., Tsujino, H., Nakano, H.,
504   Kiss, A. E. & Danabasoglu, G., 2020b. JRA55-do-based repeat year forcing datasets for
505   driving ocean–sea-ice models. *Ocean Modell.*, 147, 101557
506 Swart, N.C. & J.C. Fyfe, 2012: Observed and simulated changes in the Southern Hemisphere
507   surface westerly wind-stress, *Geophys. Res. Lett.,* 39, L16711, doi:10.1029/2012GL05281
508 Tanhua, T., D. W. Waugh, & J. L. Bullister, 2013: Estimating changes in ocean ventilation from
509   early 1990s CFC-12 and late 2000s SF6 measurements, *Geophys. Res. Lett.,* 40, 927–932,
510   doi:10.1002/grl.50251.
511 Thompson DWJ, Solomon S, Kushner PJ, England MH, Grise KM, Karoly DJ. 2011: Signatures
512   of the Antarctic ozone hole in Southern Hemisphere surface climate change. *Nat. Geosci.* 4,
513   471–479
514 Thompson, D. W. J., and J. M. Wallace (2000), Annular modes in the extratropical circulation: I.
515   Month-to-month variability, *J. Climate*, 13, 1000 – 1016.
516 Ting, Y.H. & Holzer, M., (2017) Decadal changes in Southern Ocean ventilation inferred from
517   deconvolutions of repeat hydrographies. *Geophysical Research Letters*.
518 Waugh, D.W. (2014). Changes in the ventilation of the southern oceans, *Philosophical
519   Transactions A.,* 373, 0130269.
520 Waugh, D.W and Haine, T.W.N. (2020) How rapidly do the southern subtropical oceans respond
521   to wind stress changes? *Journal of Geophys. Res.- Oceans*, to appear
522 Waugh, D. W., F. Primeau, T. DeVries, & M. Holzer (2013) Recent changes in the ventilation of
523   the southern oceans, *Science*, 339, 568.

524   Waugh, D.W., A. McC. Hogg, P Spence, M. H. England, T. W.N. Haine, 2019: Response of
525   Southern Ocean ventilation to changes in mid-latitude westerly winds, *J Climate*, 32, 5345-
526   5361.

527

528
529
530
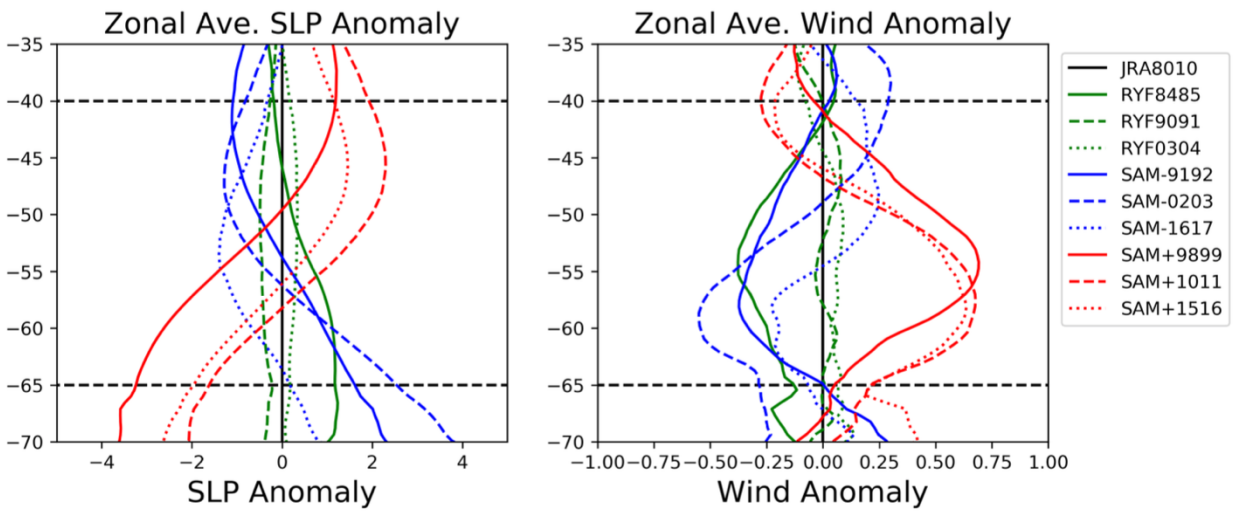
531
532 Figure 1: Latitudinal variation of anomalies in (a) sea-level pressure and (b) zonal-mean wind for
533 different years. Green curves correspond to reference years, red to positive SAM, and blue to
534 negative SAM.
535

536
537
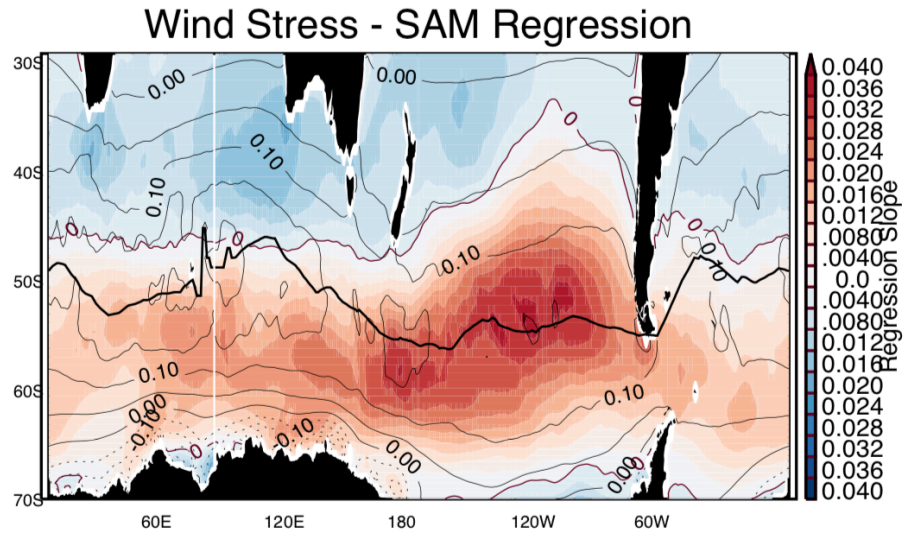
538
539
540   Figure 2: Map of linear regression coefficient between zonal wind stress and SAM index
541   (N/m²/unit SAM). Contours show climatological wind stress, and the thick curve is the location
542   of peak wind stress.
543
544

545
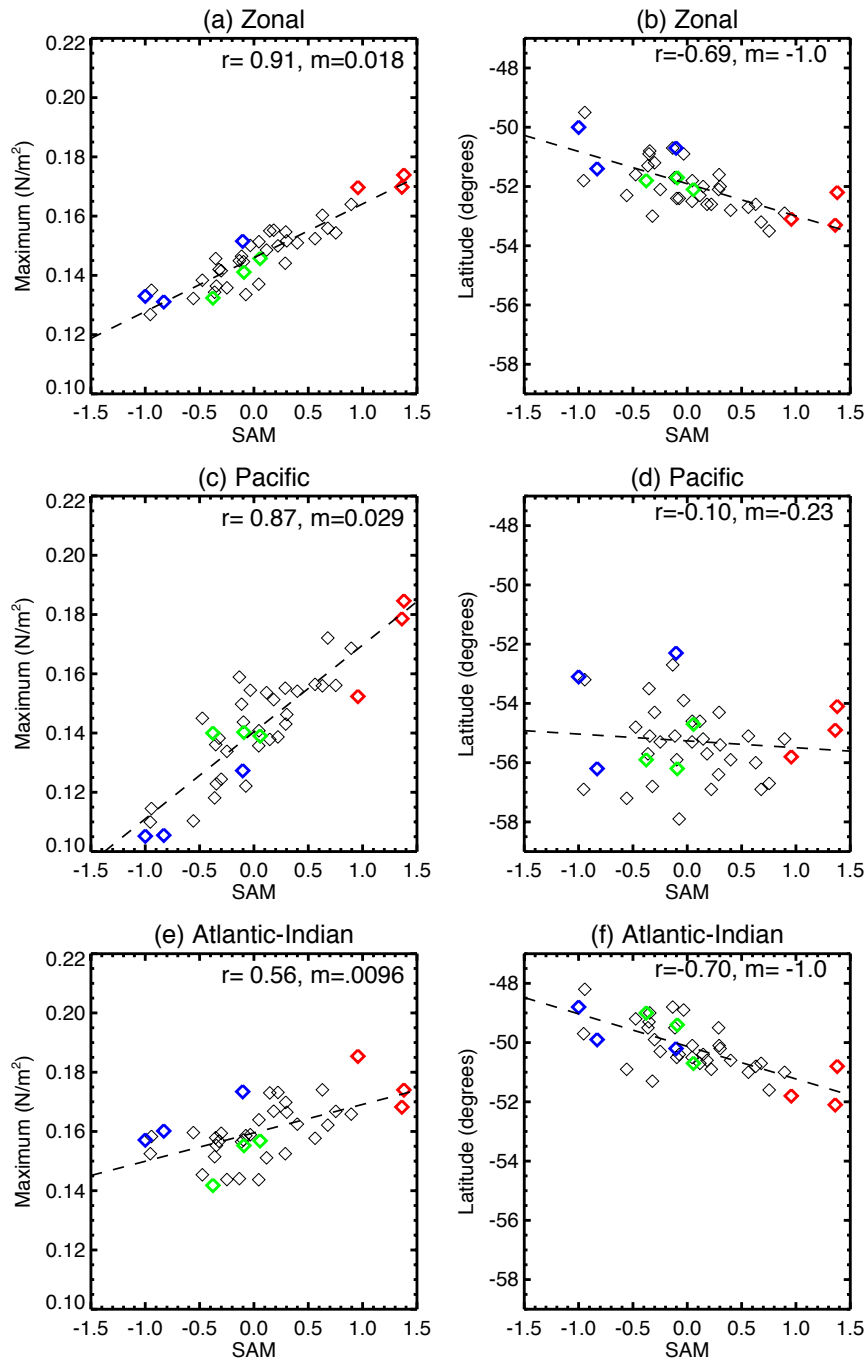
546
547 Figure 3 Scatter plots showing relationships between magnitude of peak wind stress and latitude
548 of peak wind stress with the SAM index for (a-b) zonal-mean, (c-d) Pacific-mean and (e-f)
549 Atlantic-Indian mean. Colored symbols for the RYF, SAM+ and SAM- years, as in Figure 1.
550
551

552
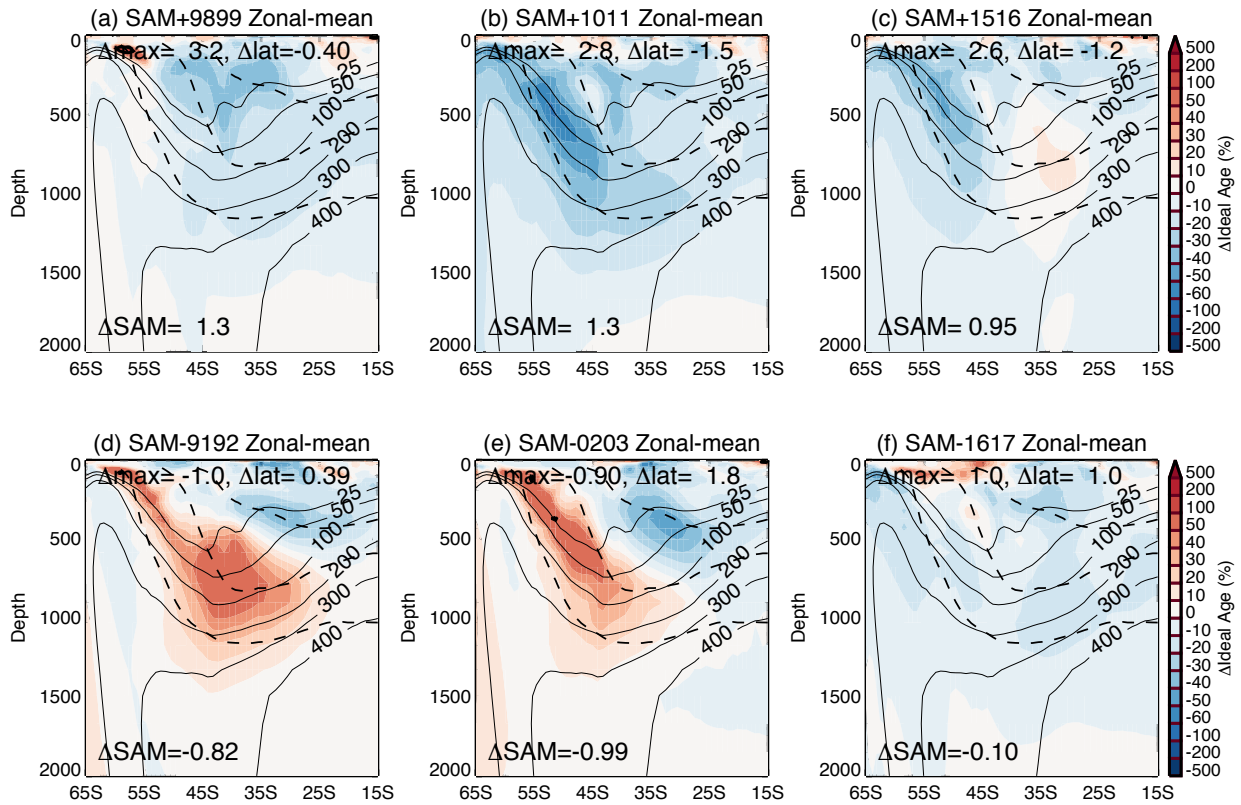
553
554 Figure 4 Depth-latitude variation of the percentage change in zonal-mean ideal age for (a-c)
555 SAM+ and (d-f) SAM- perturbations from RYF9091. Solid contours show RYF9091 ideal age,
556 and dashed contours show isopycnal surfaces. ΔSAM is the difference in SAM index between
557 perturbation and RYF simulation, Δmax the difference in maximum wind stress multipled by
558 100, and Δlat the difference in latitude of the maximum wind stress.
559
560
561
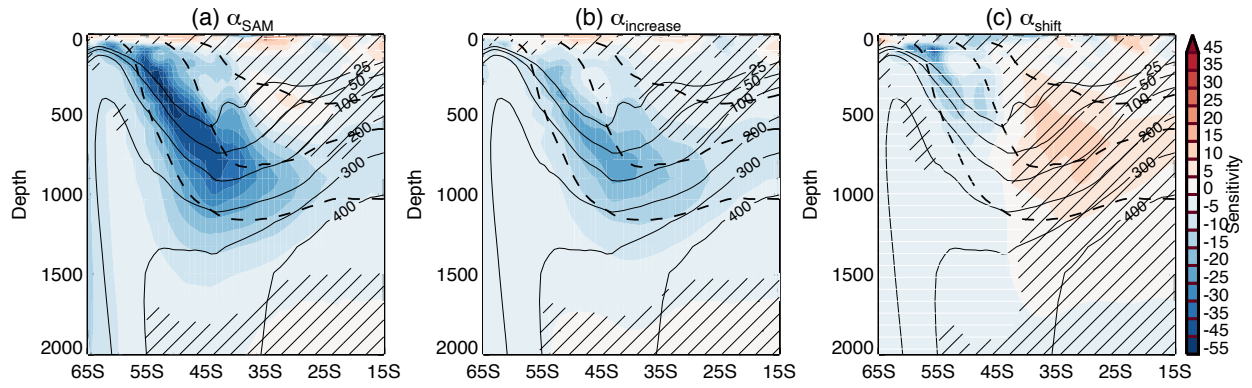
562
563 Figure 5: Depth-latitude variation of the sensitivity of the zonal-mean age to (a) an increase in
564 SAM (α_{SAM}), (b) an increase in peak wind stress ($\alpha_{increase}$), and (c) a poleward movement of the
565 peak wind stress (α_{shift}). Units are year/unit SAM, year/0.1N/m^2, and year/1° for α_{SAM}, $\alpha_{increase}$,
566 α_{shift} respectively. Contour lines as in Figure 4.   Hatching indicates regions where the
567 correlations are not significant at the 95% confidence level, using standard t-test.
568
569
570
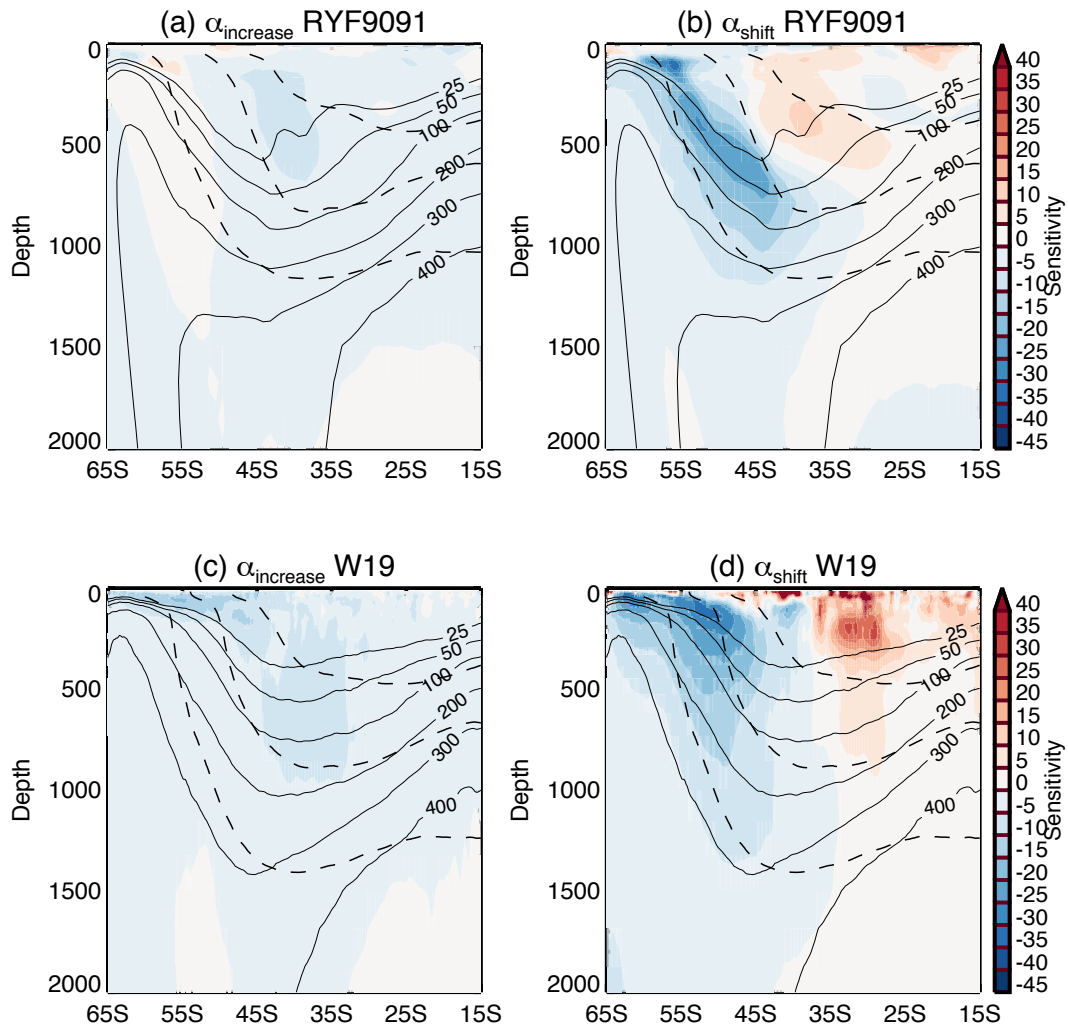
571
572 Figure 6 As in Fig 5b, c except for (a,b) RYF9091 experiments at yr 50-59, and (b) Waugh et al.
573 (2019) wind stress perturbations.
574
575

576
577
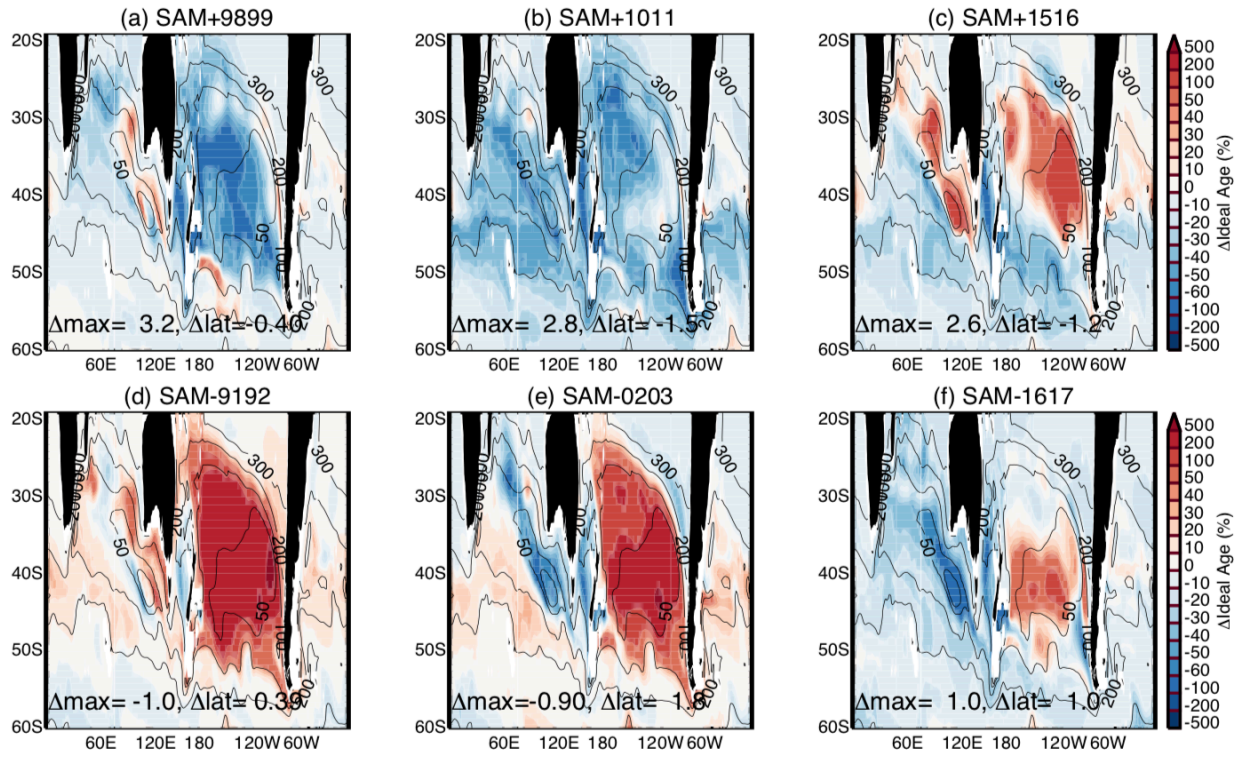
578
579 Figure 7: Maps of percentage change in age at 900 m for (a-c) SAM+ and (d-f) SAM-
580 perturbations from RYF9091. Contours show climatological age in RYF9091. Δmax and Δlat are
581 as defined in Figure 4.

582
583
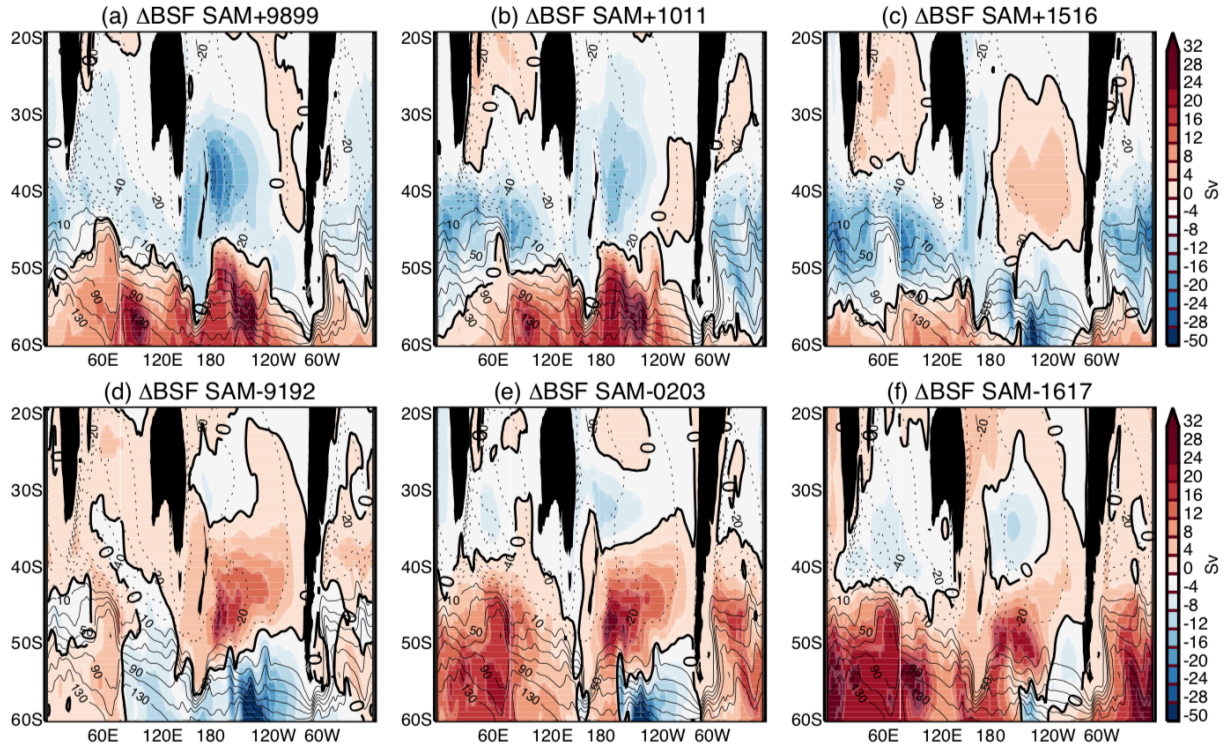
Figure 8: Maps of change in barotropic stream function (BSF) for (a-c) SAM+ and (d-f) SAM-perturbations from RYF9091. Contours show climatological BSF in RYF9091.

590
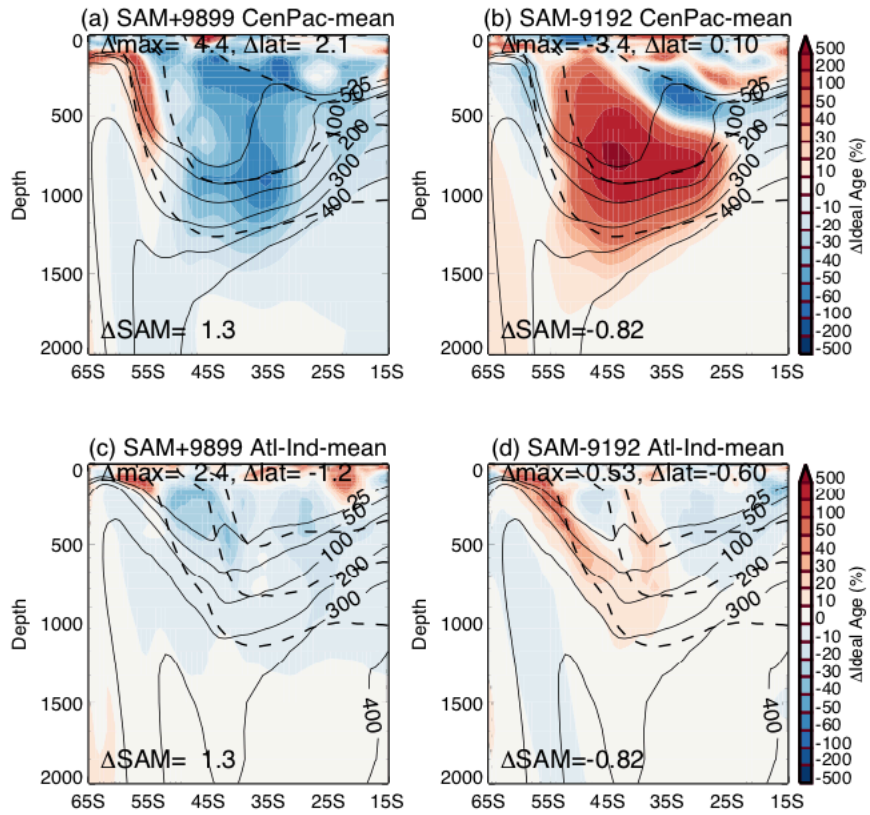
591
592 Figure 9: As in Figure 4 except for the age averaged over the (a-b) Central Pacific and (c-d)
593 Atlantic-Indian oceans, and for SAM+9899 and SAM-9192 perturbations from RYF9091.
594

595
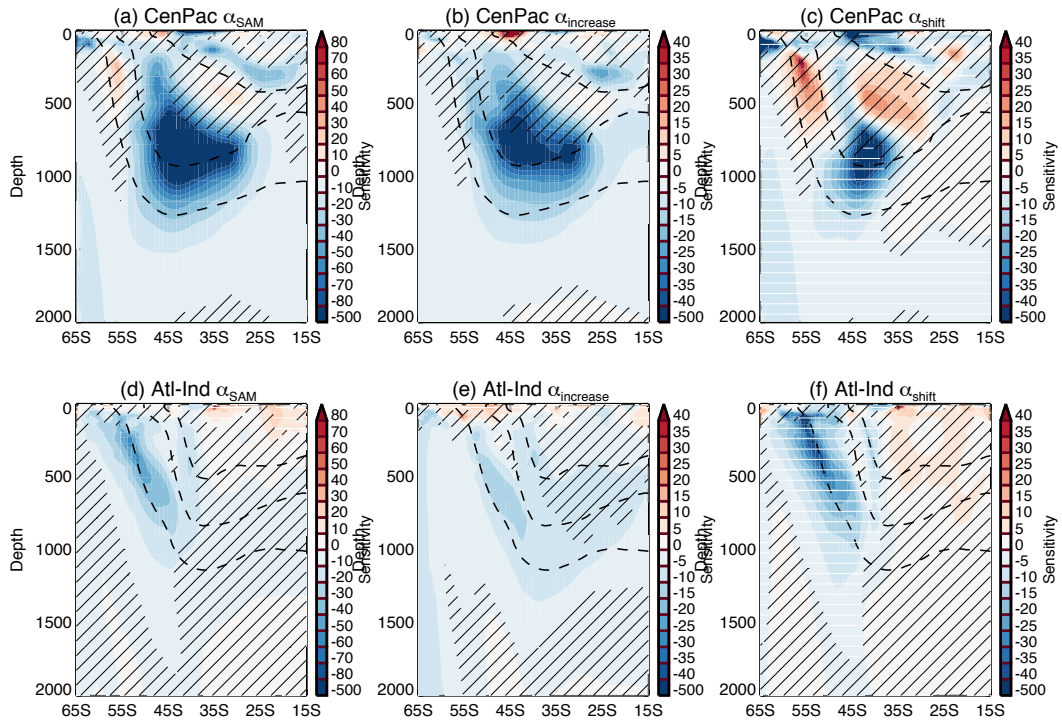
596
597   Figure 10: As in Figure 5a except for the age averaged over the (a) Central Pacific and (b)
598   Atlantic-Indian oceans.
599
600

601
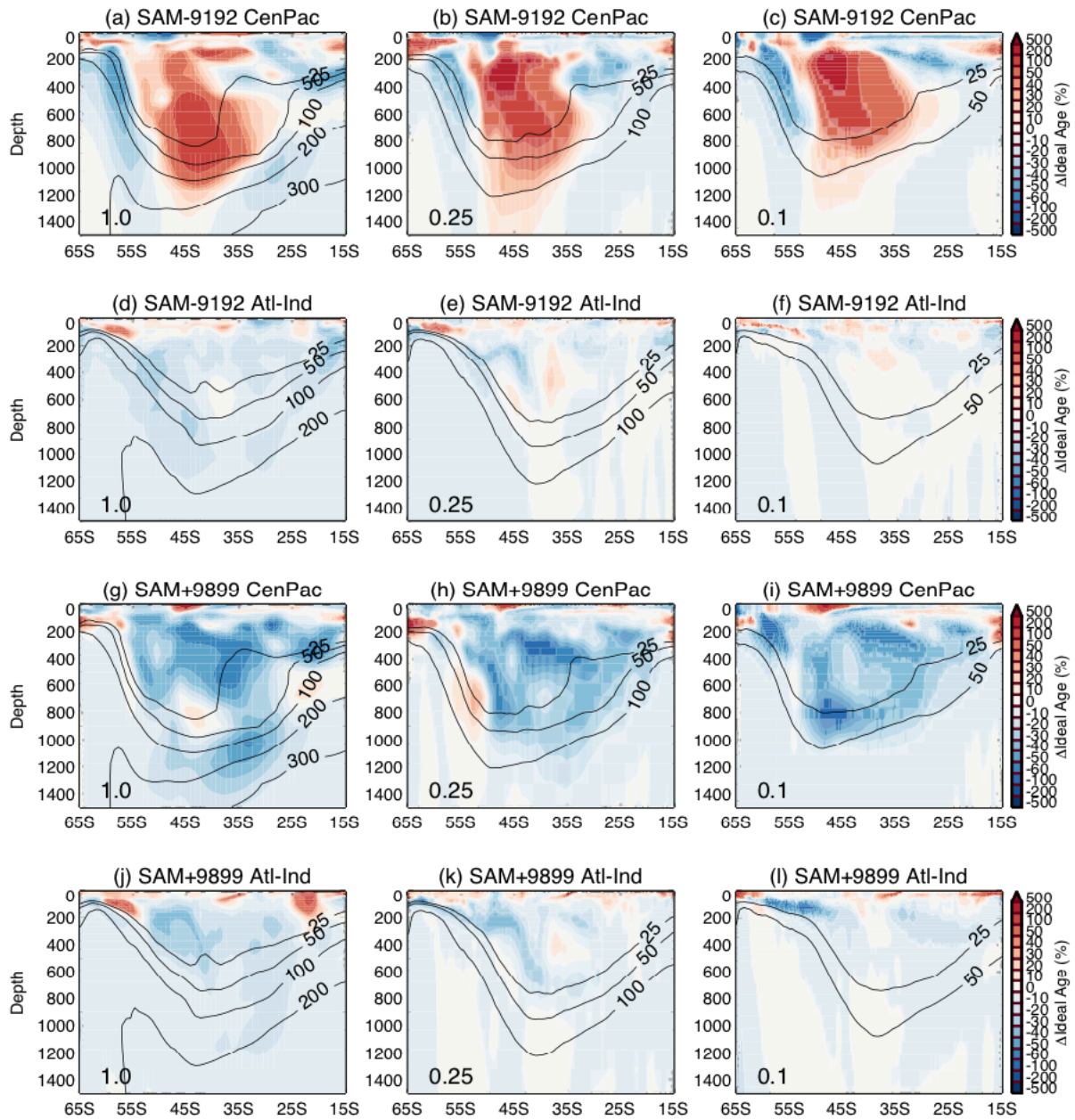
Figure 11 As in Figure 9 except showing the percentage change after 20 years for (left column) 1.0° , (middle) 0.25° and (right) 0.1° resolution simulations. Panels (a)-(f) show SAM-9192 and (g)-(l) SAM+9899 perturbations from RYF9091.